Hindawi Publishing Corporation
Journal of Nanomaterials
Volume 2014, Article ID 676908, 7 pages
http://dx.doi.org/10.1155/2014/676908

Research Article

A First Principle Comparative Study on Chemisorption of H_2 on C_{60}, C_{80}, and $Sc_3N@C_{80}$ in Gas Phase and Chemisorption of H_2 on Solid Phase C_{60}

Hongtao Wang,[1,2] Lijuan Chen,[2] Yongkang Lv,[2] Jianwen Liu,[3] and Gang Feng[4]

[1] *College of Environmental Science and Engineering, Taiyuan University of Technology, Taiyuan, Shanxi 030024, China*
[2] *Key Laboratory of Coal Science and Technology of Shanxi Province and Ministry of Education, Taiyuan University of Technology, Taiyuan, Shanxi 030024, China*
[3] *National Supercomputing Center in Shenzhen, Shenzhen 518055, China*
[4] *Shanghai Research Institute of Petrochemical Technology SINOPEC, Shanghai 201208, China*

Correspondence should be addressed to Yongkang Lv; lykang@tyut.edu.cn and Jianwen Liu; liujw@nsccsz.gov.cn

Received 11 December 2013; Accepted 13 January 2014; Published 10 March 2014

Academic Editor: Wen Zeng

The chemisorptions of H_2 on fullerenes C_{60} and C_{80}, endofullerene $Sc_3C@C_{80}$ and solid C_{60} were comparatively studied. A chain reaction mechanism for dissociative adsorption of H_2 on solid C_{60} is proposed under high pressure. The breaking of H–H bond is concerted with the formation of two C–H bonds on two adjacent C_{60} in solid phase. The adsorption process is facilitated by the application of high pressure. The initial H_2 adsorption on two adjacent C_{60} gives a much lower barrier 1.36 eV in comparison with the barrier of adsorption on a single C_{60} (about 3.0 eV). As the stereo conjugate aromaticity of C_{60} is destructed by the initial adsorption, some active sites are created. Hence the successive adsorption becomes easier with much low barriers (0.6 eV). In addition, further adsorption can create new active sites for the next adsorption. Thus, a chain reaction path is formed with the initial adsorption dominating the whole adsorption process.

1. Introduction

From the beginning of the "fullerene area," hydrogenated fullerenes have attracted wide-spread attention due to their potential application. It may not only be interesting for hydrogen storage [1–5], but also be used as an additive for lithium ion cells to significantly prolong the lifetime of these cells [6].

Experimentally, studies on the interaction between hydrogen and fullerenes have been focused on the chemical process of hydrogenation, with the products $C_{60}H_X$ and $C_{70}H_X$ being of fundamental interest as a model for other fullerene derivatives [7, 8]. A variety of chemical procedures have been devised to produce hydrogen radicals that could adsorb readily on these carbon atoms, using either reducing reagents [1, 9, 10], or catalysts [11]. In addition, direct hydrogenation of C_{60} and C_{70} has also been achieved without the usage of a catalyst by exposing solid-phase fullerenes to high-pressure hydrogen gas (0.5–30 kB) at elevated temperature (500–600 K) [4].

Theoretically, hydrogen storage based on fullerene materials has attracted many attentions. Using first principle calculations based on density functional theory, Sun and coworkers reported that each $B_{36}C_{36}$ cage can store at most 18 hydrogen molecules at zero temperature [12]. They also find that an isolated $Li_{12}C_{60}$ cluster where Li atoms are capped onto the pentagonal faces of the fullerene not only is very stable but also can store up to 120 hydrogen atoms in molecular form with a binding energy of 0.075 eV/H_2 [13]. Zhao and coworkers report that a particular Scandium organometallic buckyballs can bind as many as 11 hydrogen atoms per transition metal, which gives the maximum retrievable H_2 storage density 9 wt% [14]. Kang and coworkers reports that Ni-dispersed fullerenes are considered to be capable of

storing 6.8 wt% H_2, with H_2 desorption activation barrier of 11.8 kcal/mol, which is ideal for many practical hydrogen storage [15].

However, the mechanism for direct reactions between H_2 and these fullerenes remains unexplained to the best of our knowledge. Chan et al. proposed the mechanism of H_2 molecule dissociative chemisorption on the close cousin of fullerenes, carbon nanotubes, in solid phase under high pressure [16]. The breaking of the H–H bond is concerted with the formation of two C–H bonds on two adjacent carbon nanotubes in solid phase, facilitated by the application of high pressure which shortens the interstitial distance between nanotubes. The adsorption behavior gives some hints on H_2 adsorption on fullerenes.

In this work, we proposed a chain reaction mechanism for H_2 molecules dissociative adsorption on solid C_{60} under high pressure. In comparison, we also studied H_2 adsorption on the most stable fullerenes C_{60} and C_{80} in gas phase as well as endofullerene $Sc_3N@C_{80}$.

2. Computational Method

The first principles total energy and electronic structure calculations were carried out within the framework of DFT [17] with a plane wave basis set and pseudopotentials for the atomic cores, as implemented in the Vienna ab initio simulation package (VASP) [18, 19]. The PW91 gradient correction was added to the local density exchange-correlation functional and projector augmented wave (PAW) pseudopotentials [20, 21] were employed, with an energy cutoff of 400 eV for the plane-wave expansion as these approaches have successfully applied to similar systems [16]. The supercell is sampled with a $1 \times 1 \times 1$ k-points mesh, generated by the Monkhorst-Pack algorithm. The convergence criteria were 1.0×10^{-4} eV for the SCF energy, 1×10^{-3} eV for total energy, and 0.05 eV/Å for atomic force, respectively.

A climbing image nudged elastic band method was used to locate the transition states [22–24]. The vibrational frequencies and normal modes were calculated by diagonalization of the mass-weighted force constant matrix, which was obtained using the method of finite differences of forces as implemented in VASP. The ions are displaced in the +/– directions of each Cartesian coordinate by 0.02 Å. There is only one imaginary frequency for all these structures, indicating that they are indeed the transition states in the potential energy surface.

The adsorption energies (E_{ads}) for the adsorption of H_2 on fullerenes were calculated by

$$E_{ads} = E(\text{fullerence} + H_2) - [E(\text{fullerene}) + E(H_2)], \quad (1)$$

where E(fullerene + H_2), E(fullerene), and $E(H_2)$ are the total energies of H_2 adsorbed fullerene, total energies of fullerene (fullerene = C_{60}, C_{80}, $Sc_3N@C_{80}$), and the total energies of H_2, respectively. The larger adsorption energy indicates the stronger adsorption.

Table 1: Energy barriers and reaction energies (ΔE) for H_2 adsorption on C_{60}, C_{80} and $Sc_3N@C_{80}$ in gas phase. Energies are given in eV.

	Absorption site	Barrier (eV)	ΔE (eV)
C_{60}	6-6 parallel	3.68	−0.87
	6-6 perpendicular	3.57	−0.86
	5-6 parallel	3.04	−0.10
	5-6 perpendicular	3.05	−0.09
C_{80}	6-6 parallel	2.47	−0.50
	6-6 perpendicular	2.47	−0.50
	5-6 parallel	2.26	−1.10
	5-6 perpendicular	2.27	−1.10
$Sc_3N@C_{80}$	Sc non-bonded C	3.60	−0.14
	Sc bonded C	3.78	−0.04

3. Results and Discussion

3.1. H_2 Adsorption in Gas Phase. We firstly consider the H_2 adsorption on fullerenes C_{60} and C_{80} and endofullerene $Sc_3N@C_{80}$ to explore the possible adsorption media without any catalyst in gas phase. In the calculations, the interactions between H_2 molecule and fullerenes (or endofullerenes) were modeled in a supercell of size 16.0 Å × 16.0 Å × 16.0 Å, with one k-point (gamma point). The energy barriers and reaction energies are listed in Table 1.

3.1.1. H_2 Adsorption on C_{60} in Gas Phase. The icosahedral C_{60} consists of 12 pentagons and 20 hexagons. Hence the bonds can be categorized as two types, pentagon-hexagon bonds (5-6 bond) and hexagon-hexagon bonds (6-6 bond). Addition on adjacent sites such as 5-6 bond and 6-6 bond engenders isomers. Furthermore, addition can take place on nonadjacent sites, which would produce many isomers. For $C_{60}H_2$, the simplest fullerene dihydride, there are 23 isomers. However, there is only one isomer that has been characterized. Among all kinds of $C_{60}H_2$ isomers, (1,2) addition products are considered as the most stable. To compare the adsorption difference, we investigated H_2 adsorption on both 5-6 and 6-6 bonds. In addition, two adsorption modes are considered. One case is that the H–H bond of incoming H_2 is to be considered to parallel the 6-6 bond (Structure A and Structure E in Figure 1). The other one is that the incoming H–H bond is to be considered to point perpendicularly to the C–C bond (Structure C and Structure G in Figure 1). Energetically, the total exothermic energy for the formation of the two C–H bonds in 6-6 bond addition production is 0.77 eV favorable than that for 5-6 bond addition (Table 1), indicating that 6-6 bond addition gives the most stable structure. The two adsorption modes result in two possible adsorption mechanisms. The parallel adsorption mode gives a concerted mechanism, in which two H atoms bonded to two C atoms (TS 1 in Figure 1), respectively. In contrast, the perpendicular adsorption mode gives a step mechanism (one H atom is adsorbed first, then the second one, TS 2 in Figure 1). The barriers for both concerted mechanism and step mechanism are so high that the reaction is very difficult

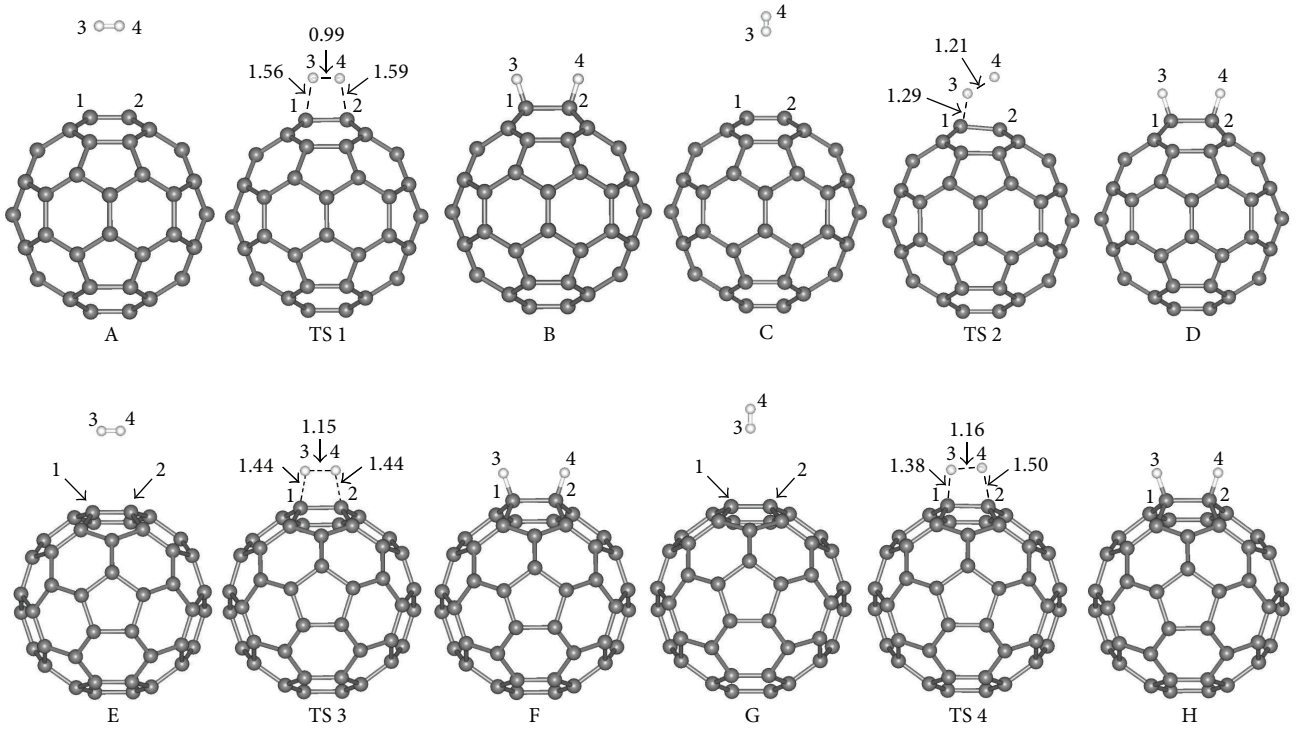

FIGURE 1: Structures and transition states structures for H_2 molecule adsorption on C_{60} in gas phase. Selective distances are given in Å.

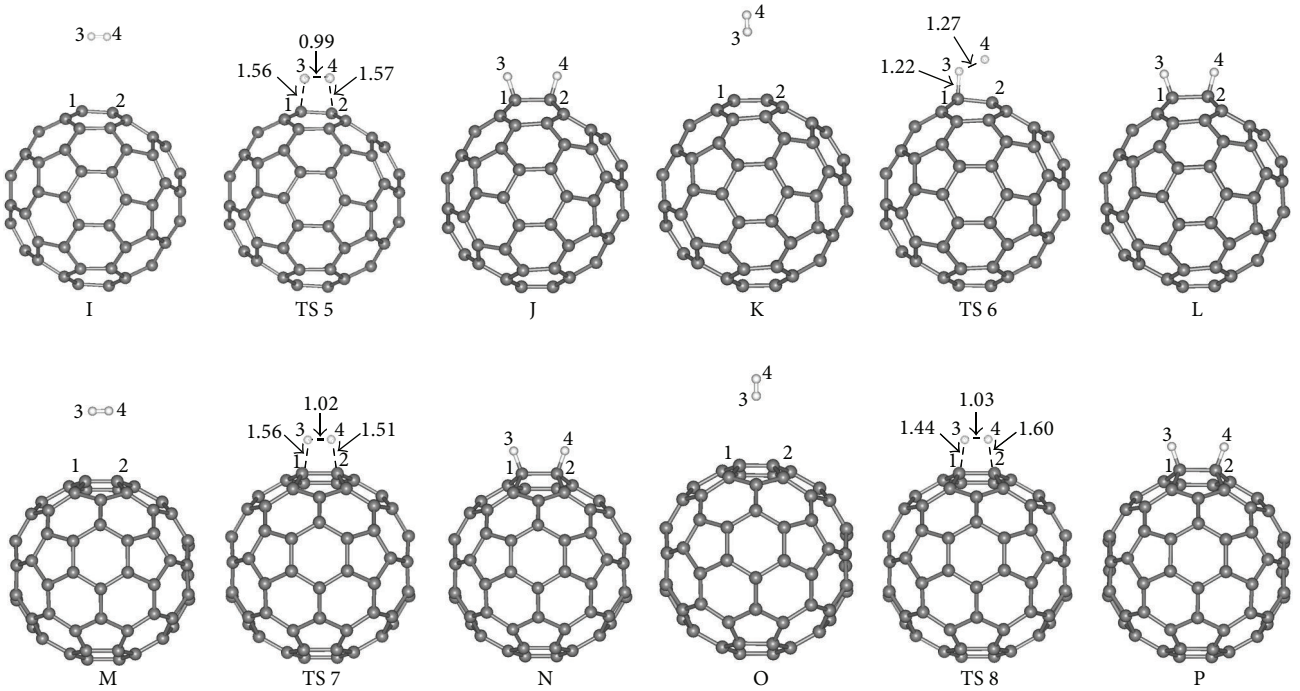

FIGURE 2: Optimized structures and transition states structures for H_2 molecule adsorption on C_{80} in gas phase. Selective distances are given in Å.

to take place, although the barrier for the step mechanism is 0.11 eV favorable than that for the concerted mechanism.

3.1.2. H_2 Adsorption on C_{80} in Gas Phase. C_{80} has the same I_h symmetry as C_{60}, so it can also be served as adsorption media, although experimentally no hydrite of C_{80} has been characterized. We carried out the same calculations as we did on C_{60} as shown in Figure 2. The 6-6 parallel and perpendicular adsorption modes have the same energy barrier of 2.47 eV whereas 5-6 parallel and perpendicular adsorption

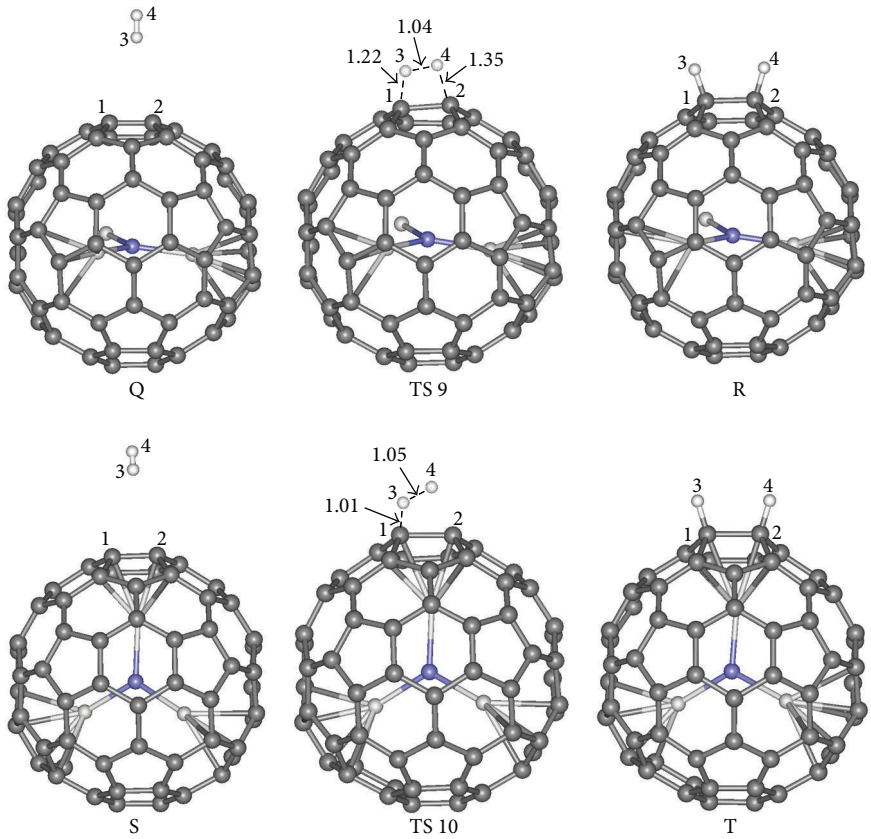

Figure 3: Optimized structures and transition states structures for H_2 molecule adsorption on $Sc_3N@C_{80}$ in gas phase. Selective distances are given in Å.

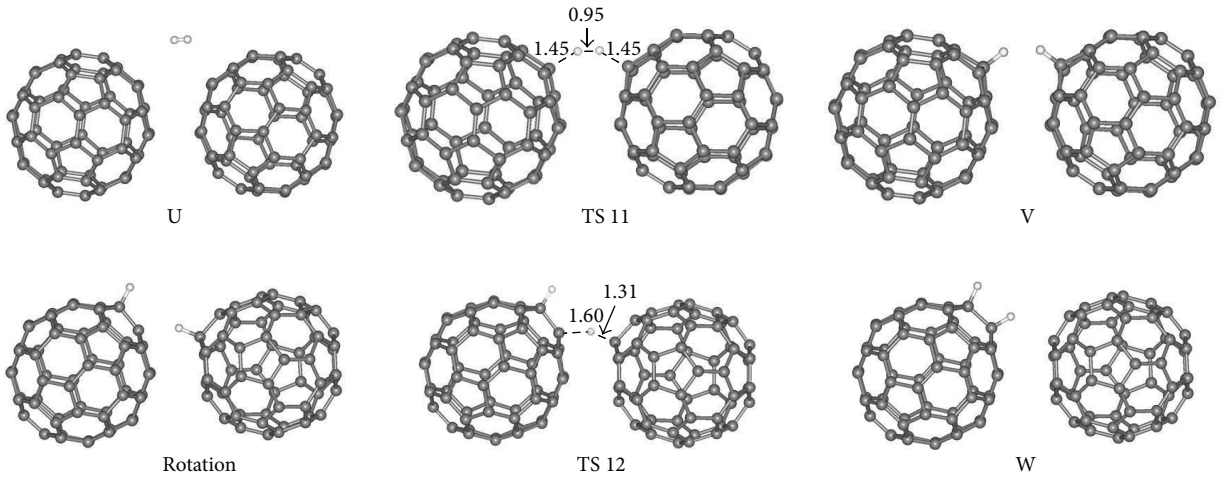

Figure 4: Optimized structures and transition state (TS) structures for the first H_2 dissociative chemisorption on solid C_{60} array. Selective distances are given in Å.

modes have the same barrier of 2.27 eV. Comparing to that of C_{60}, the calculated energy barrier is about 1 eV lower than that for C_{60} due to the less stability of C_{80}.

3.1.3. H_2 Adsorption on $Sc_3N@C_{80}$ in Gas Phase. As one of the most stable endofullerene, $Sc_3N@C_{80}$ has become accessible in macroscopic quantities. Since the adsorption barrier for C_{80} has decreased more obviously than that for C_{60}, its stable derivative $Sc_3N@C_{80}$ is expected to be a promising hydrogenation material. As shown in Figure 3, we considered two different adsorption modes: either adsorption to Sc bonded C or Sc nonbonded C. However, whichever atom H bonds, the calculated energy barriers are more

Table 2: Reaction barriers and reaction energies (ΔE) for the second H_2 absorption on solid C_{60} with three different absorption modes.

Absorption site	Barrier (eV)	ΔE (eV)
(1,2)-(1,2)	0.76	−2.05
(1,2)-(1,4)	0.59	−1.82
(1,4)-(1,4)	0.52	−1.81
Former absorption	1.21	−1.77

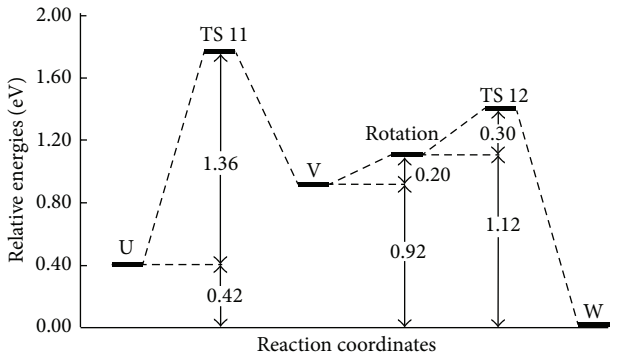

Figure 5: Reaction profile for the adsorption of the first H_2 on solid C_{60} array. Energies are given in eV.

than 3.5 eV, indicating that $Sc_3N@C_{80}$ can hardly react with H_2. In addition, the overall exothermic energy is quite low at 0.1 eV, indicating that the reaction is not very favorable thermodynamically.

3.2. H_2 Adsorption in Solid Phase. In contrast, the solid phase, composed of bundles of C_{60}, provides a unique chemical environment dependent on the external pressure and makes it much easier for H_2 dissociative chemisorption on C_{60} bucky balls. In our calculations, the interactions between hydrogen molecule H_2 and C_{60} were modeled in a supercell of size 9.55 Å × 9.55 Å × 13.50 Å, and an external pressure of ~50 kB was introduced.

3.2.1. Adsorption of the First H_2 on Solid C_{60}. Under the pressure of pressure of ~50 kB, we explored the reactive trajectory of the first H_2 dissociative chemisorption on C_{60} as shown in Figure 4. There are three steps involved: first, the incoming H_2 dissociation and deposition on two adjacent C_{60}, from structure U to V, through transition structures (TS 11); second, the rotation of C_{60}; and finally, hydrogen migration through TS 12 to structure W, a 1,2-addition product. Figure 5 gives the plot of the relative energies for the dissociative H_2 chemisorption on solid C_{60}. From this figure, we can see that the initial dissociative chemisorption step has a barrier of 1.36 eV, while the barrier for the subsequent H migration is much lower at 0.5 eV. Compared to adsorption barrier on single C_{60} in gas phase, the barrier for H_2 molecules adsorption on two adjacent C_{60} is quite low at 1.36 eV, which indicates that the reaction can easily take place at room temperature [16]. The energy barrier differences are mainly due to the rotation. In high pressure, C_{60} does not stand in his own position quietly but rotates around the center of mass randomly. The rotation deforms the H–H bond to help break the H–H bond, which leads to lower reaction barrier.

In addition, we have made some comparison between the first H_2 chemisorption on solid C_{60} and solid (6,6) armchair carbon nanotube. The barrier difference for initial chemisorption is 0.14 eV. And the barrier difference for the H atom migration is 0.38 eV. Both the barrier differences are small. From this table, we can conclude that, energetically, there are no significant differences between the chemisorption on solid C_{60} and solid carbon nanotube under high pressure.

3.2.2. Adsorption of the Second H_2 on Solid C_{60}. To explore whether it is possible to chemisorb more H_2 on the solid C_{60} under high pressure, we investigate the reaction path for the addition of the second H_2 on C_{60} as shown in Figure 6. The reaction mechanism is quite similar to the addition of the first one. In this process, the second H_2 also dissociatively chemisorbs on two adjacent C_{60} in the initial step and then rotates slightly; one of the H atom migrates from one C_{60} to another and finally forms two 1,2-addition products. The relative energies for the chemisorption of second H_2 on solid C_{60} were shown in Figure 7. Compared to the first H_2 chemisorption, the calculated barrier for the second H_2 is 1.21 eV in the dissociation step, which is a littler lower than that for the first H_2 adsorption. In addition, the overall process is also more exothermic, from 0.44 eV to 1.77 eV. This is mainly due to the fact that the first H_2 molecule adsorption has already partially disrupted the conjugated system, so further addition is much easier.

In the first H_2 adsorption process, we have mentioned that one of the H atoms will transfer from one C_{60} radical to another. There is another probability that H_2 molecules react with the intermediate radical directly. We also investigate this kind of adsorption modes. For the $C_{60}H$ intermediate, there are two active sites: site 2 and site 4. There are three probable adsorption modes: (1,2)-(1,2) adsorption, (1,4)-(1,4) adsorption, and (1,2)-(1,4) adsorption. For (1,2)-(1,2) adsorption, it means one H atom is adsorbed in site 2 and another H atom is also adsorbed in site 2 (Figure 8). The rules also apply for both (1,2)-(1,4) adsorption and (1,4)-(1,4) adsorption. The barriers of three category reactions are listed in Table 2. From this table, we can see that all the barriers are no more than 0.8 eV. They are much lower than the formerly calculated barrier 1.21 eV. The overall exothermic energies are also a little larger than the former calculated exothermic energy 1.77 eV. Based on these data, a conclusion can be drawn that the subsequent H_2 molecules will easily react with C_{60} intermediate radicals. Thus the reaction is a chain reaction: once the first H_2 is adsorbed, the H_2 will be adsorbed one by one. There is no extra energy needed because the overall exothermic energy will compensate the energy which is needed to overcome the barrier. Herein the first H_2 molecule adsorption has become the crucial step in the overall adsorption.

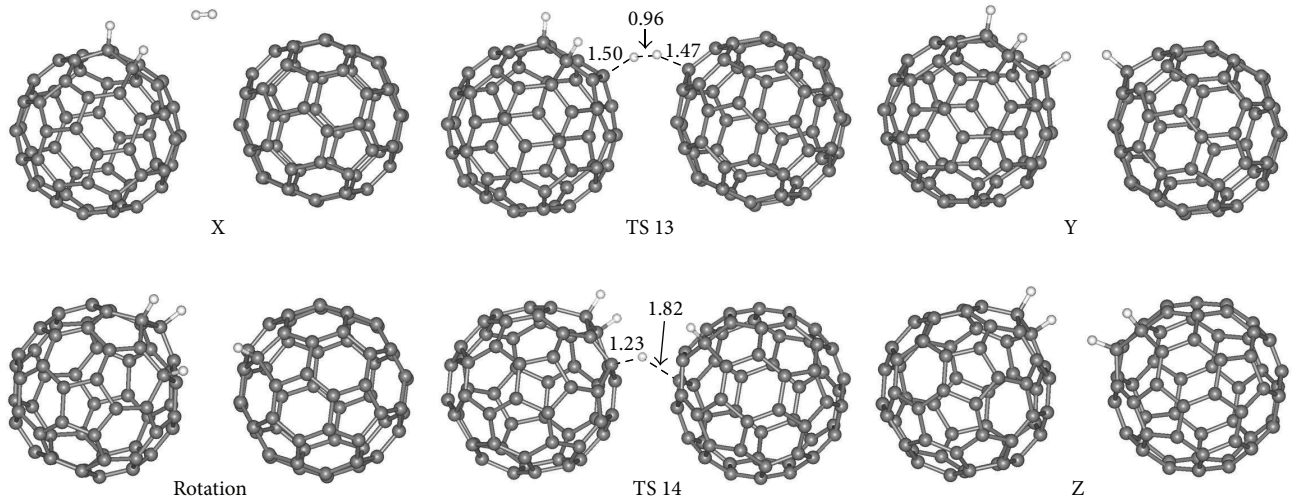

Figure 6: Optimized structures and transition state (TS) structures for the second H_2 dissociative chemisorption on C_{60}. Selective distances are given in Å.

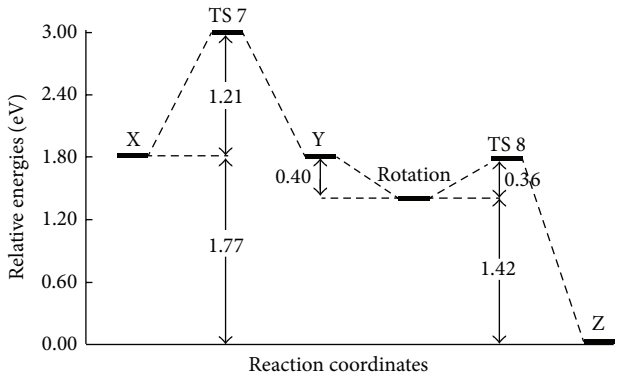

Figure 7: Reaction profile for the second H_2, dissociative chemisorption on solid C_{60}. Energies are given in eV.

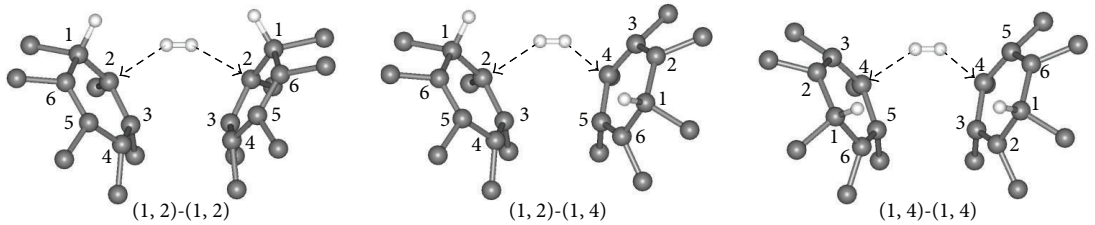

Figure 8: Adsorption modes for the second H_2 adsorption.

4. Conclusions

Based on the investigation of H_2 molecules chemisorption on fullerenes C_{60} and C_{80} and endofullerene $Sc_3C@C_{80}$, we proposed a mechanism for H_2 molecules adsorption on solid C_{60} under high pressure. Due to the rotation of C_{60}, the H_2 molecule will easily chemisorb on two adjacent C_{60} under high pressure, which is more favorable than the H_2 molecule adsorption on single C_{60}. The overall reaction is a chain reaction. The first H_2 molecules adsorption is the crucial step in the overall H_2 molecules adsorption process. Once the first H_2 molecules is adsorbed on the C_{60}, the second and subsequent H_2 will easily be adsorbed on the C_{60} due to the lower reaction barrier.

Conflict of Interests

The authors declare that there is no conflict of interests regarding the publication of this paper.

Acknowledgments

This work is supported by the Shenzhen Strategic Emerging Industries Special Fund Program of China (Grant nos. GGJS20120619101655715 and JCY20120619101655719), the Program for International Cooperation Projects of Shanxi Province (Grant no. 2010081018), and National Natural Science Foundation of China (Grant no. 51078252).

References

[1] C. C. Henderson and P. A. Cahill, "$C_{60}H_2$: synthesis of the simplest C_{60} hydrocarbon derivative," *Science*, vol. 259, no. 5103, pp. 1885–1887, 1993.

[2] Y. Ye, C. C. Ahn, B. Fultz, J. J. Vajo, and Z. Zinck, "Hydrogen adsorption and phase transitions in fullerite," *Applied Physics Letters*, vol. 77, no. 14, pp. 2171–2173, 2000.

[3] S. Ballenweg, R. Gleiter, and W. Kratschmer, "Hydrogenation of buckminsterfullerene C_{60} via hydrozirconation: a new way to organofullerenes," *Tetrahedron Letters*, vol. 34, no. 23, pp. 3737–3740, 1993.

[4] C. Jin, R. Hettich, R. Compton, D. Joyce, J. Blencoe, and T. Burch, "Direct solid-phase hydrogenation of fullerenes," *Journal of Physical Chemistry*, vol. 98, no. 16, pp. 4215–4217, 1994.

[5] A. A. Peera, L. B. Alemany, and W. E. Billups, "Hydrogen storage in hydrofullerides," *Applied Physics A: Materials Science and Processing*, vol. 78, no. 7, pp. 995–1000, 2004.

[6] A. Hirsch and M. Brettreich, *Fullerenes: Chemistry and Reactions*, Wiley-VCH, New York, NY, USA, 2005.

[7] P. A. Cahill and C. M. Rohlfing, "Theoretical studies of derivatized buckyballs and buckytubes," *Tetrahedron*, vol. 52, no. 14, pp. 5247–5256, 1996.

[8] C. C. Henderson, C. McMichael Rohlfing, and P. A. Cahill, "Theoretical studies of selected $C_{60}H_2$ and $C_{70}H_2$ isomers," *Chemical Physics Letters*, vol. 213, no. 3-4, pp. 383–388, 1993.

[9] R. E. Haufler, J. Conceicao, L. P. F. Chibante et al., "Efficient production of C_{60} (buckminsterfullerene), $C_{60}H_{36}$, and the solvated buckide ion," *Journal of Physical Chemistry*, vol. 94, no. 24, pp. 8634–8636, 1990.

[10] C. C. Henderson, C. M. Rohlfing, K. T. Gillen, and P. A. Cahill, "Synthesis, isolation, and equilibration of 1,9- and 7,8-$C_{70}H_2$," *Science*, vol. 264, no. 5157, pp. 397–399, 1994.

[11] L. Becker, T. P. Evans, and J. L. Bada, "Synthesis of $C_{60}H_2$ by rhodium-catalyzed hydrogenation of C_{60}," *Journal of Organic Chemistry*, vol. 58, no. 27, pp. 7630–7631, 1993.

[12] Q. Sun, Q. Wang, and P. Jena, "Storage of molecular hydrogen in B-N cage: energetics and thermal stability," *Nano Letters*, vol. 5, no. 7, pp. 1273–1277, 2005.

[13] Q. Sun, P. Jena, Q. Wang, and M. Marquez, "First-principles study of hydrogen storage on $Li_{12}C_{60}$," *Journal of the American Chemical Society*, vol. 128, no. 30, pp. 9741–9745, 2006.

[14] Y. Zhao, Y.-H. Kim, A. C. Dillon, M. J. Heben, and S. B. Zhang, "Hydrogen storage in novel organometallic buckyballs," *Physical Review Letters*, vol. 94, no. 15, Article ID 155504, 2005.

[15] W. H. Shin, S. H. Yang, W. A. Goddard III, and J. K. Kang, "Ni-dispersed fullerenes: hydrogen storage and desorption properties," *Applied Physics Letters*, vol. 88, no. 5, Article ID 053111, pp. 1–3, 2006.

[16] S.-P. Chan, G. Chen, X. G. Gong, and Z.-F. Liu, "Chemisorption of hydrogen molecules on carbon nanotubes under high pressure," *Physical Review Letters*, vol. 87, no. 20, Article ID 205502, 2001.

[17] R. Car and M. Parrinello, "Unified approach for molecular dynamics and density-functional theory," *Physical Review Letters*, vol. 55, no. 22, pp. 2471–2474, 1985.

[18] G. Kresse and J. Furthmüller, "Efficient iterative schemes for ab initio total-energy calculations using a plane-wave basis set," *Physical Review B*, vol. 54, no. 16, pp. 11169–11186, 1996.

[19] G. Kresse and J. Furthmüller, "Efficiency of ab-initio total energy calculations for metals and semiconductors using a plane-wave basis set," *Computational Materials Science*, vol. 6, no. 1, pp. 15–50, 1996.

[20] P. E. Blöchl, "Projector augmented-wave method," *Physical Review B*, vol. 50, no. 24, pp. 17953–17979, 1994.

[21] G. Kresse and D. Joubert, "From ultrasoft pseudopotentials to the projector augmented-wave method," *Physical Review B*, vol. 59, no. 3, pp. 1758–1775, 1999.

[22] G. Henkelman and H. Jónsson, "Improved tangent estimate in the nudged elastic band method for finding minimum energy paths and saddle points," *Journal of Chemical Physics*, vol. 113, no. 22, pp. 9978–9985, 2000.

[23] G. Henkelman and H. Jónsson, "Improved tangent estimate in the nudged elastic band method for finding minimum energy paths and saddle points," *Journal of Chemical Physics*, vol. 113, no. 22, pp. 9978–9985, 2000.

[24] G. Henkelman, B. P. Uberuaga, and H. Jónsson, "Climbing image nudged elastic band method for finding saddle points and minimum energy paths," *Journal of Chemical Physics*, vol. 113, no. 22, pp. 9901–9904, 2000.